

1 **Title**

2

3 *Full title:*

4

5 Commuting-driven competition between transmission chains shapes seasonal influenza
6 virus epidemics in the United States

7

8 *Short title:*

9

10 Dynamics of influenza virus spread in the USA

11

12 **Authors**

13

14 Simon P.J. de Jong,¹ Andrew Conlan,² Alvin X. Han,^{1†} Colin A. Russell^{1†*}

15

16 **Affiliations**

17

18 ¹Department of Medical Microbiology & Infection Prevention, Amsterdam University
19 Medical Centers, University of Amsterdam; Amsterdam, The Netherlands.

20 ²Department of Veterinary Medicine, University of Cambridge; Cambridge, United
21 Kingdom.

22

23 † Contributed equally

24 *Corresponding author. Email: c.a.russell@amsterdamumc.nl

25

26 **Abstract**

27 Despite intensive study, much remains unknown about the dynamics of seasonal influenza
28 virus epidemic establishment and spread in the United States (US) each season. By
29 reconstructing transmission lineages from seasonal influenza virus genomes collected in
30 the US from 2014 to 2023, we show that most epidemics consisted of multiple distinct
31 transmission lineages. Spread of these lineages exhibited strong spatiotemporal hierarchies
32 and lineage size was correlated with timing of lineage establishment in the US. Mechanistic
33 epidemic simulations suggest that mobility-driven competition between lineages
34 determined the extent of individual lineages' geographical spread. Based on
35 phylogeographic analyses and epidemic simulations, lineage-specific movement patterns
36 were dominated by human commuting behavior. These results suggest that given the
37 locations of early-season epidemic sparks, the topology of inter-state human mobility
38 yields repeatable patterns of which influenza viruses will circulate where, but the
39 importance of short-term processes limits predictability of regional and national epidemics.

40 **Teaser**

41

42 Epidemics consist of multiple sub-epidemics that compete for susceptible hosts and
43 spread due to the movement of commuters.

44

45 MAIN TEXT

46

47 Introduction

48

49

50

51

52

53

54

55

56

57

58

59

In the United States, seasonal influenza epidemics recur every year as the result of a complex hierarchy of transmission processes. Intercontinental viral migration, driven by global metapopulation dynamics, drives the initial early-season seeding of epidemics in the US (1–3). Following these initial epidemic sparks, inter-state patterns of human mobility disseminate viruses across the country (4–9), resulting in an interconnected network of local epidemics (10, 11). These epidemics vary substantially from year to year in their timing, size, and composition (12–14). Gaining a predictive understanding of the variables that shape the composition, timing and magnitude of these epidemics is a key public health target (15). Substantial efforts have been put into forecasting the timing of epidemic onset and epidemic peaks to aid public health planning (14, 16–21).

60

61

62

63

64

65

66

67

68

69

70

71

72

73

Knowledge of the underlying transmission processes that give rise to epidemic establishment and subsequent spread is essential for a predictive understanding of epidemic characteristics (22, 23). For example, does peak-period epidemic activity arise from the gradual expansion of early-season transmission chains, or are epidemics the result of transmission chains that rapidly expanded when conditions became favorable for large-scale transmission? Similarly, do epidemics tend to comprise a single epidemic wave that sweeps across country, or rather do they consist of many co-circulating transmission lineages that jointly shape epidemics (24, 25)? Further questions remain regarding the underlying mobility drivers of viral spread, such as the roles of air travel and commuting in disseminating viruses country-wide (4–6, 26). The US forms a particularly compelling setting to explore fundamental questions about the determinants of influenza virus spread due to its geographical expanse, climatic variability and complex mobility networks.

74

75

76

77

78

79

80

81

82

83

84

Most previous studies into seasonal influenza epidemic dynamics in the US have relied primarily on virological and syndromic surveillance data, such as pneumonia and influenza (P&I) mortality data or influenza-like illness (ILI) data (4–6). However, such data cannot effectively distinguish between distinct chains of transmission, potentially limiting the precision and specificity with which the underlying dynamics of epidemic establishment and viral migration can be reconstructed (4, 23). Hence, we turned to genomic data, collected during routine surveillance in the United States. By decomposing epidemics into contributions of individual transmission lineages and reconstructing their individual spread, we aimed to gain more fine-grained insight into the processes of epidemic establishment and spread.

85

86

87

88

89

90

91

92

93

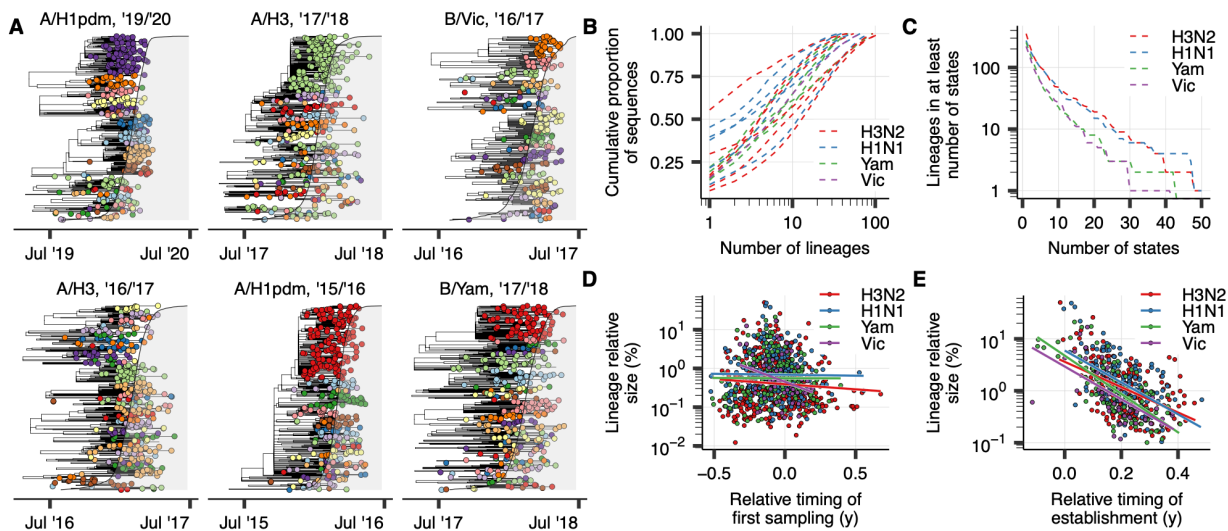
94

85 Results

Influenza virus epidemics consist of many distinct co-circulating transmission lineages

First, we characterized the transmission lineage structure of US seasonal influenza epidemics. We investigated whether epidemics tend to comprise many distinct co-circulating transmission lineages that independently emerged in different states, or rather consist of a single dominant transmission lineage that propagates across the country. We analyzed 30,508 whole-genome seasonal influenza virus sequences from the 48 contiguous states and the District of Columbia, collected during routine surveillance in

95 the United States from 2014 to 2023, the most recent period for which substantial whole-
96 genome sequences were available. In this period, all four influenza A subtypes/influenza
97 B lineages (henceforth, subtypes) caused epidemic activity, but patterns of subtype
98 dominance differed substantially from season to season (Fig. S1). To classify the viruses
99 circulating in each season into transmission lineages, we phylogenetically grouped the
100 viruses into clusters of viruses that exhibit a comb-like branching structure, suggestive of
101 exponential spread (27). Given the exponential nature of influenza virus epidemics, we
102 posit that groups of viruses with such a rapidly expanding branching structure plausibly
103 represent groups of viruses that expanded from a single ancestral virus in the United
104 States (Fig. 1A, S2-5).



106 **Fig. 1: Lineage structure of US seasonal influenza epidemics.**

107 (A) Phylogenies of six representative subtype-season pairs, with tips colored by
108 identified transmission lineage. The shaded grey area corresponds to the cumulative
109 proportion of nation-wide positive tests in public health laboratories of the corresponding
110 subtype at each point in time.

111 (B) The size distribution of lineages by season and subtype. Each line represents the
112 cumulative proportion of sequences that is accounted for by a number of lineages on the
113 x-axis. Each line corresponds to an individual season, for an individual subtype.

114 (C) The number of lineages across that accounts for >5% of sequences in a season-
115 subtype in at least the number of states on the x-axis, by subtype.

116 (D) Relationship between the first collection date of virus in a lineage and the lineage's
117 country-wide size normalized by state. Lineage sampling dates were computed relative to
118 the timing of nation-wide epidemic onset, which was defined as the first week in which
119 >5% of the season's cumulative positive tests had been collected.

120 (E) Relationship between the timing of establishment of substantial circulation of a
121 lineage and its country-wide size normalized by state. Lineage establishment timing was
122 computed relative to nation-wide epidemic onset analogous to (D).

123
124

125 Using this procedure, we clustered 81.2% of sequences into 3,842 lineages of at least two
126 viruses. In most seasons, a relatively small number of transmission lineages accounted
127 for the bulk of sequenced viruses (Fig. 1B), with the median minimum number of
128 lineages that together accounted for at least 50% of sequences amounting to 5 lineages
129 (range 1-13) across all seasons for subtypes that accounted for >10% of positive tests in
130 the respective season. The degree of lineage diversity differed substantially across
131 seasons (Fig. 1B). For example, in the 2015/2016 A/H1N1pdm09 epidemic, a single
132 transmission lineage accounted for >50% of sequenced viruses, normalized across states.
133 In contrast, in the 2016/2017 A/H3N2 season, the largest lineage accounted for only
134 6.4% of sequenced viruses. Lineage structure was evident for both circulating influenza
135 A virus subtypes and both influenza B virus lineages, though transmission lineage
136 clustering results are likely more error-prone for influenza B viruses given their lower
137 evolutionary rate (28), particularly in seasons that saw relatively little circulation and
138 were less densely sampled.

140 Consistent with the lineage size distribution, most transmission lineages were confined to
141 a relatively small number of states, with a small proportion of lineages spreading widely
142 across the country (Fig. 1C): among the 1,104 identified transmission lineages that
143 accounted for at least 5% of sequences in a season in at least one state, 144 (13.0%)
144 lineages did so in at least 10 states, and 27 (2.4%) did so in at least 25. Patterns of lineage
145 diversity at the state level mirrored those at the national level, with some seasons seeing
146 very high within-state lineage diversity (e.g. 2018/2019 A/H1N1pdm09, median state-
147 wise Shannon entropy of lineage composition = 0.76, inter-quartile range 0.68-0.82),
148 whereas in other seasons a few lineages dominated state-level epidemics (e.g. 2018/2019
149 A/H3N2, median Shannon entropy = 0.44, inter-quartile range = 0.31-0.58). These
150 results indicate that in most seasons, seasonal influenza epidemics are the result of the
151 co-circulation of multiple independent chains of transmission, consistent with previous
152 studies into individual seasons, both at the national and state level (24, 25).

153 *Lineage size correlates with timing of establishment but not emergence*

155 Next, we investigated the factors that influence the extent to which any individual
156 transmission lineage will spread country-wide. We hypothesized that onset timing would
157 explain the substantial variation in lineage size, where the first lineages to emerge in any
158 season, for any subtype, would be larger. Here, we defined lineage size as the proportion
159 of sequences that a lineage accounts for in a season for a subtype across all states, where
160 each state has an equal weight. However, across all subtypes and seasons, we found that
161 a relationship between time of first sampling of a lineage and (log) lineage size was weak
162 (Spearman $\rho = -0.07$, $P = 0.024$) (Fig. 1D). We observed the proliferation of some
163 transmission lineages that were first sampled a substantial amount of time prior to onset
164 of nation-wide epidemic activity, but many of the most successful lineages emerged and
165 were first sampled relatively close in time to the ramp-up of national epidemic activity
166 (Fig. 1D).

168 For example, by the time of first sampling of the largest lineage in the highly severe (29)
169 2017/2018 season (Fig. 1A, topmost lineage), >10% of all the season's sequences had
170 already been collected. Despite its relatively late emergence, the lineage accounted for
171 >40% of sequences during peak epidemic periods following rapid expansion. These
172 rapidly expanding lineages could in some cases descend from unsampled viruses that had
173 circulated prior locally at low levels, but the fact that a single ancestral virus could
174

175 rapidly sweep to national dominance despite emerging at a time when many other
176 transmission lineages already circulated suggests that early-season transmission
177 processes are highly heterogeneous. Furthermore, the fact that the lineages dominating
178 during peak epidemic periods often rapidly expanded around the time of epidemic onset,
179 outcompeting co-circulating low-level transmission lineages, indicates that in many
180 seasons very short-term epidemiological processes are crucial determinants of seasonal
181 influenza epidemic dynamics.

182
183 The weak correlation between timing of first lineage sampling and lineage size suggests
184 that early-season transmission chains frequently go extinct before the onset of substantial
185 epidemic activity. However, we hypothesized that if a lineage did cause substantial
186 epidemic activity early on, it would be well-positioned to be successful country-wide.
187 Correspondingly, we found that the timing of establishment of substantial epidemic
188 activity of a transmission lineage correlated strongly with nation-wide lineage size
189 (Spearman $\rho = -0.53$, $P < 0.001$) (Fig. 1E). Here, we defined the timing of lineage
190 establishment as the first week in which the lineage accounted for substantial epidemic
191 activity (i.e. at least 5% of total estimated incidence in the season; see Materials and
192 Methods) in at least one state. The fact that the lineages that first established substantial
193 epidemic activity somewhere in the US were more likely to be successful country-wide
194 suggests that the states with the earliest epidemic onset have outsized contributions to
195 nationwide epidemic lineage composition.

196 197 *Transmission lineages are highly spatially structured*

198
199 To investigate the extent to which transmission lineages are spatially structured, we
200 computed the Bray-Curtis similarity index of epidemic transmission lineage
201 compositions for all pairs of states. Here, states that more frequently sampled viruses
202 belonging to the same transmission lineages have a higher similarity index. Aiming to
203 identify communities of states that are more closely linked to one another than to other
204 states, we performed hierarchical clustering on the similarity matrices. Qualitatively, this
205 clustering recapitulated the geography of the United States, with relatively higher
206 similarity for states within the same census region (Fig. 2A). Projecting the similarities
207 among states onto a two-dimensional surface further recapitulated this spatial structure;
208 for example, states belonging to the Northeast and Southeast appeared to form distinct
209 clusters (Fig. 2B). However, the continuous distribution of states on the plane suggests
210 states cannot consistently be classified into distinct communities, suggestive of
211 substantial inter-regional mixing.

212
213 Consistent with the states' clustering by geography, we found that epidemics in states in
214 closer geographic proximity more frequently comprised the same transmission lineages
215 (Mantel test, $P < 0.001$) (Fig. 2C). The highest similarity indices were found for
216 neighboring states (highest: MS-LA, MO-KS, GA-AL, NH-MA, UT-ID), with a
217 neighboring state being the state with the highest similarity in 81% (34/42) of states
218 included in the analysis. Stratifying by season and subtype, this correlation between
219 distance and similarity (Mantel test, $P < 0.01$) was present in almost all (14/15) subtype-
220 season pairs that accounted for >10% of nation-wide positive tests in their respective
221 season. Together, these results show that at the transmission lineage level, US seasonal
222 influenza epidemics are highly spatially structured.

223

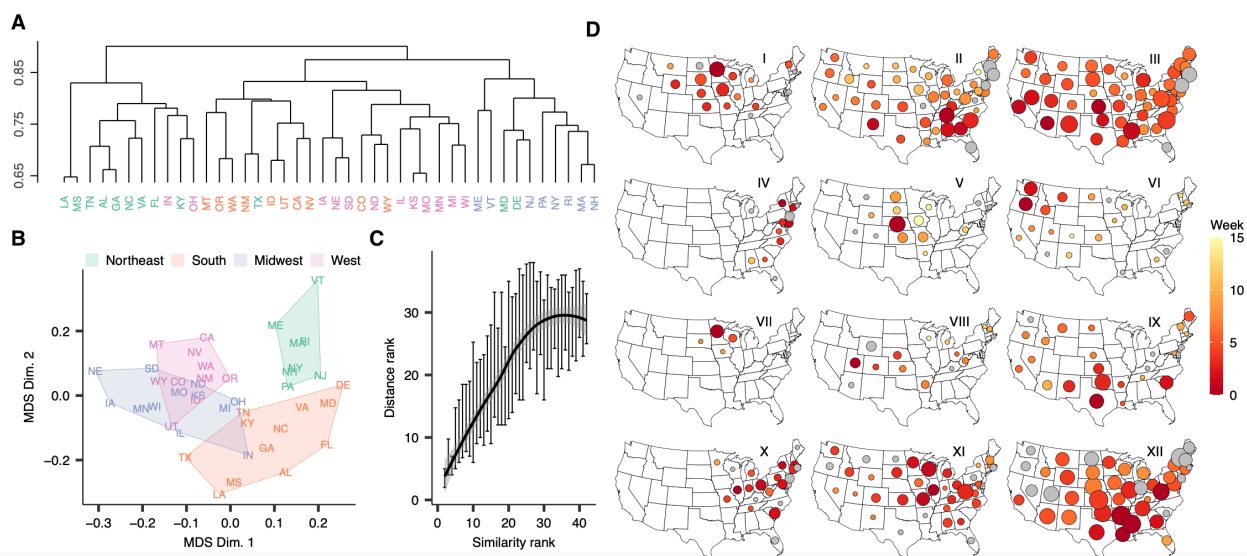


Fig. 2: Spatial structure of US seasonal influenza epidemics.

(A) Complete-linkage hierarchical clustering of pairwise state-to-state transmission lineage composition Bray-Curtis similarities across all subtypes, colored by census region.

(B) Multi-dimensional scaling plot of the pairwise lineage composition Bray-Curtis similarity among states, colored by census region.

(C) Relationship between pairwise transmission lineage compositional similarity and pairwise centroid distance rank. Vertical lines show 50% CI for each value of rank similarity, line corresponds to LOESS fit to medians.

(D) Examples of lineage spatiotemporal spread. In each map, circle size and color correspond to the relative size and establishment timing of the corresponding lineage in each state, respectively. Grey fill corresponds to unknown lineage establishment timing.

To further investigate the spatiotemporal dynamics of viral spread, we reconstructed the spread of individual transmission lineages. We mapped the sampling dates of the viruses in each lineage to epidemiological data to quantify, in each state, 1) the relative size of each lineage, defined as the proportion of all viruses of that subtype that was accounted for by the lineage in that season; and 2) the week of lineage establishment, defined as the first week the lineage accounted for substantial levels of circulation in that state (i.e. at least 5% of total estimated incidence in the season; see Materials and Methods). We visualized lineage spread by projecting the timing of establishment and size of the lineage in each state on a map. These visualizations revealed a striking landscape of seasonal influenza spatial spread at the transmission lineage level, with examples for a geographically and temporally representative set of lineages shown in Fig. 2D. We identified instances of lineage emergence from all regions of the US, each with distinct signatures of spread. Across seasons and subtypes, many lineages exhibited a radial spatiotemporal progression and were highly regional (e.g. I, V, VI, VII, Fig. 2D); other lineages saw rapid cross-country spread (e.g. II, III, XII, Fig. 2D).

Consistent source-sink dynamics are absent across seasons and subtypes

The above results suggest that lineages can potentially emerge in any region of the United States. We sought to more rigorously investigate seasonal influenza virus source-sink dynamics at the transmission lineage level for all seasons and subtypes by

260 identifying each lineage's most likely origin state. We performed discrete trait
261 phylogeographic reconstructions for each lineage individually in BEAST (30),
262 identifying the Health & Human Services (HHS) region that represented the most likely
263 region of initial expansion for each of the 262 transmission lineages that accounted for
264 >0.5% of sampled viruses, normalized by state, in their respective season. To ensure our
265 results were robust to differences in sampling across regions, we performed these
266 analyses with two distinct subsampling strategies: first, one where the number of
267 sequences included for each HHS region depended on its population size; and second,
268 one with a constant number of sequences across HHS regions. We found substantial
269 season-to-season variation for the most probable origin regions for successful lineages.
270 Of the seven transmission lineages that accounted for >10% of sequences in a single
271 season, normalized across states, three likely first established in the South (HHS regions
272 4 & 6; e.g. lineages II & XII, Fig. 2D), one likely emerged in the West (HHS region 9;
273 lineage III, Fig. 2D), one in the Midwest (HHS regions 7 & 5; lineage XI, Fig. 2D), one
274 in the Northeast (HHS region 1), and one could not consistently be attributed to a single
275 region across both sampling strategies.

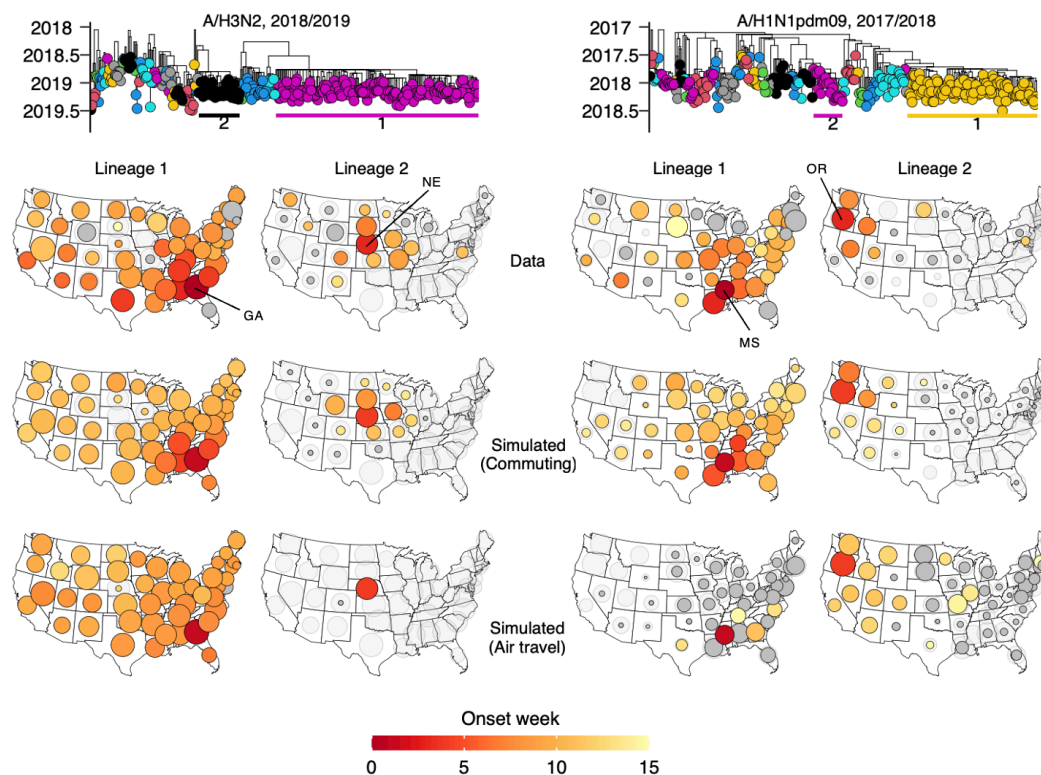
276
277 With the aim of identifying regional variation in source-sink dynamics, we computed
278 state-specific origin profiles that quantify the role of each HHS region as the region of
279 initial lineage expansion of sampled viruses in each state. These profiles differed
280 substantially across states (Fig. S6, S7). For example, averaged across both subsampling
281 strategies, the proportion of sequences reconstructed to coalesce to epidemic expansions
282 in HHS region 4, encompassing most of the Southeast, ranged from 39.3% in South
283 Carolina (HHS region 4) and 27.4% in Arkansas (HHS region 6) to 13.0% in Arizona
284 (HHS region 8). Similarly, lineages expanding in HHS region 10, encompassing the
285 Pacific Northwest, accounted for 15.3% of sampled viruses in Idaho (HHS region 10),
286 10.7% in North Dakota (HHS region 8), and only 2.7% in Arkansas (HHS region 6).
287 States in closer geographic proximity saw more similar origin profiles, even if they
288 corresponded to different HHS regions (Mantel test, $P < 0.001$). Across all states, a
289 relatively limited proportion of viruses corresponded to lineages that originated from the
290 state's own HHS region (median 17.3%, range 11.4%-29.8% for uniform subsampling
291 strategy), suggesting a high degree of viral mixing at the national level. Importantly,
292 origin profiles were strongly correlated across the two subsampling strategies (Spearman
293 $\rho = 0.81$, $P < 0.001$). Together, these results suggest that influenza virus source-sink
294 dynamics are highly heterogeneous, without consistent source regions of successful
295 lineages, but are spatially structured.

296 *Mechanistic simulations suggest commuting flows drive viral spread*

297
298
299 Our analyses established a strong correlation between timing of lineage establishment
300 and lineage size (Fig. 1E). However, this correlation does not account for a substantial
301 portion of the observed variation in transmission lineage size. We hypothesized that
302 differences in mobility flows, coupled to inter-lineage competition, could explain why
303 some lineages spread widely following local establishment, whereas other lineages
304 remain highly spatially constrained. Importantly, the reconstructed spread of individual
305 lineages provided a vital ground truth which we could leverage to resolve long-standing
306 questions regarding the underlying mobility determinants of influenza virus spread.

307
308 The lineage competition hypothesis appears to explain lineage dynamics in the
309 2018/2019 A/H3N2 season. The beginning of this season was dominated by

310 A/H1N1pdm09 viruses, but it also saw the rapid expansion of viruses of the A/H3N2
 311 subtype that were associated with decreased vaccine effectiveness (31). Phylogenetic
 312 analyses, integrated with epidemiological data, indicate that A/H3N2 circulation in this
 313 season was dominated by two lineages, appearing to emerge from Georgia (GA, lineage
 314 1) and Nebraska (NE, lineage 2), respectively (Fig. 3, left), each establishing swiftly as
 315 evidenced by a comb-like, rapid branching structure. Visualizations of the lineages’
 316 distributions across states suggest that spread of the Nebraskan lineage was regional and
 317 radial, causing substantial epidemic activity mainly in the immediately surrounding states
 318 in a clear spatiotemporal hierarchy (Fig. 3, left). Conversely, the lineage from Georgia
 319 quickly spread to almost all states with a less prominent temporal hierarchy, although it
 320 appeared to arrive in neighboring states first. We hypothesized that competition from the
 321 Georgian lineage explained why spread of the Nebraskan lineage remained so regional.
 322 In turn, this would explain why the Georgian lineage failed to spread substantially in
 323 Nebraska and immediately surrounding states.



326
 327 **Fig. 3: Mobility drivers of influenza virus spread.**

328 Phylogenies represents the 2018/2019 A/H3N2 season (left) and 2017/2018
 329 A/H1N1pdm09 season (right), with the two largest lineages labeled in each. For both
 330 seasons, the maps in the top row visualize the reconstructed spread of the labeled
 331 lineages, with size and color corresponding to lineage size and establishment timing, in
 332 each state, respectively. Middle maps show simulated spread of the two lineages for each
 333 of the two seasons, using commuting data, when initialized in their origin state in their
 334 likely origin week. Bottom maps are analogous to the middle maps but using air travel
 335 data instead of commuting data. Light grey circles represent the total proportion of
 336 sequences in that state that are accounted for by the lineages that were simulated, to
 337 account for the fact that simulations only incorporated a subset of all lineages; circles for
 338 the simulated lineages have their size scaled such that the sum of simulated lineages’

339 sizes for each state is proportional to the proportion of sequences accounted for by the
340 simulated lineages in that state (i.e., the light grey area). Dark grey fill corresponds to
341 absence of an establishment week (for top row, potentially due to missing data), or
342 establishment after the 15th week.

343
344 To test the hypothesis that competitive interactions between lineages, coupled to
345 mobility, drive lineage spread, we explored if we could reproduce the spread of these two
346 lineages in mechanistic epidemic simulations. To do so, we used a metapopulation model
347 that models viral spread between states in a susceptible-infected-recovered (SIR)
348 epidemic framework. The model simulates the spread of multiple co-circulating lineages
349 that compete for disease-susceptible individuals with perfect cross-immunity between
350 transmission lineages. We initialized the simulations in the lineages' respective
351 establishment weeks, in their respective onset states (Georgia and Nebraska) and
352 simulated forward in time to model the spread of the two lineages. By visualizing which
353 of the two lineages would predominate in each state in the simulations, we could
354 ascertain if we could reproduce their observed spread. To ascertain the predominant
355 mobility drivers of viral spread, we parameterized rates of state-to-state mobility using
356 either commuting flows, extracted from the US Census Bureau, or air travel data,
357 extracted from the US Department of Transportation.

358
359 When using rates of commuting to parameterize rates of inter-state travel, we could
360 reproduce the observed spread of the two lineages with striking accuracy: the simulations
361 recapitulated the radial spread from Nebraska, and the relative success of the lineage
362 emerging from Georgia (Figure 3, left). The simple model of inter-lineage competition
363 driven by commuting also explains why the lineage from Georgia failed to cause
364 epidemic activity in the Nebraska and the immediately surrounding states. On the other
365 hand, the correspondence to observed spread was very poor when using air travel flows,
366 with an absence of substantial spread from Nebraska. Together, these mechanistic
367 simulations suggest that commuting flows were the primary correlate of viral spread.
368 These results also support the notion that competitive interactions between lineages,
369 mediated by mobility flows, shape the distribution of lineages across states.

370
371 *Spatial segregation and limited competition allow lineages from small states to spread*
372 *widely*

373
374 The 2018/2019 A/H3N2 season lends genome-informed credence to the conjectured
375 gravity-like spread of seasonal influenza viruses (5), with a lineage originating from a
376 populous, highly connected state (in this case, Georgia, population ~11 million)
377 spreading quickly through strong long-range connections, while spread from a smaller
378 state (Nebraska, population ~2 million) was slower and more local. Georgia's high
379 degree of connectivity and earlier onset allowed lineage 1 to spread to other states more
380 rapidly than lineage 2, with its day of arrival in another state on average 42 days (IQR
381 27-53) earlier than lineage 2's in metapopulation simulations. Nevertheless, the
382 substantial spread of the Nebraskan lineage shows that spatial segregation between
383 lineages can allow a lineage emerging from a small state to proliferate, even if it co-
384 circulates with a lineage emerging from a more populous state, as long as it sees
385 sufficiently early establishment and is spatially segregated from the lineage emerging
386 from the larger state.

388 Our results suggests that by facilitating spread from less populous states, the short-range
389 spatial coupling reflected in commuting flows is a key determinant of seasonal influenza
390 virus spread. This notion is further supported in the 2017/2018 A/H1N1pdm09 season, in
391 which the two largest lineages appeared to emerge in Mississippi (MS) and Oregon (OR),
392 respectively (Fig. 3, right). When using commuting flows, the relative degree of spread
393 of the two lineages could be reproduced. Despite its relatively small population,
394 Mississippi's high connectivity through commuting flows allowed lineage 1 to rapidly
395 spread beyond local constraints. In contrast, due to Oregon's relatively limited
396 connectivity and the later establishment of lineage 2, competition from lineage 1 likely
397 constrained the spread of those viruses to the Western United States. When using only air
398 travel to parameterize inter-state mobility, the simulations strongly overestimated the
399 degree of spread from Oregon relative to Mississippi, with too slow spread from
400 Mississippi, compared to the ground truth (Fig. 3, right).

402 Using counterfactual simulations, we explored how mobility interacts with establishment
403 timing to competitively shape the spread of individual lineages. Under the baseline
404 simulations for the 2018/2019 A/H3N2 season, lineage 2 accounted for >10% of
405 circulation among the two lineages in 11 states. Simulations indicate that had lineage 2
406 established in Nebraska four weeks later (with lineage 1's establishment timing
407 unchanged), lineage 2 would have accounted for >10% of circulation in only 4 states,
408 constrained by competition from lineage 1. Conversely, if it had established four weeks
409 earlier, lineage 2 would have been accounted for >10% of circulation in 37 states,
410 spreading much more extensively (Fig. S8). Similarly, in the 2017/2018 A/H1N1pdm09
411 season, later onset for lineage 2 would have constrained it to the Pacific Northwest,
412 whereas earlier onset would have facilitated substantially more expansive spread (Fig.
413 S9).

414 *Mobility patterns coupled to inter-lineage competition explain differences in lineages'* 415 *spread*

418 To further test the capacity of mobility-mediated inter-lineage competition to explain
419 individual lineages' spread, we performed in-depth investigations into the 2019/2020
420 B/Victoria season, which was characterized by anomalously high amounts of epidemic
421 activity (32) and a highly spatially diverse lineage composition, with the largest lineages
422 appearing to originate in or in the vicinity of California (lineage 1), Florida (lineage 2),
423 Texas (lineage 3), Louisiana (lineage 4), Nevada (lineage 5), and Washington (lineage 6),
424 respectively (Fig. 4). Some lineages spread to over half of all states (e.g. lineages 1 and 2
425 from Florida and California, respectively), whereas spread was more regional for others.
426 We sought to establish if we could analogously reproduce the distribution of the lineages
427 across states using epidemic simulations.

429 Using a combination of commuting flows and air travel flows, the simulations
430 reproduced the spread of individual lineages and their distribution across states (Fig. 4).
431 Differences in mobility flows in combination with competition for susceptible
432 individuals, linked to timing of lineage establishment, parsimoniously explain why the
433 lineages emerging from California and Florida spread widely, whereas the lineages from
434 Louisiana and Washington were more spatially constrained. Commuting flows in
435 isolation provided a similarly strong fit, but underestimated spread from Nevada,
436 suggesting that residual air travel flows not captured by commuting could play a role in
437 viral dissemination (Fig. S10). Conversely, simulations using air travel deviated from the

ground truth, particularly by underestimating short-range viral migration from Louisiana and Washington (Fig. S11).

The co-circulation of many lineages across distinct regions in this season illustrates how concurrent processes of epidemic establishment in different states, interacting with mobility, mediate nation-wide epidemic lineage composition and spatial structure. This season also highlights the heterogeneity of lineage establishment processes. For example, the lineage emerging from Florida likely emerged in in the spring of 2019 (posterior mean TMRCA May 5, 95% CrI March 14 – June 12), seemingly persisting throughout the 2019 summer in Florida. Hence, this lineage potentially provides a counterexample to the general trend that viruses do not persist between seasons (24). Conversely, the lineages from California, Nevada, and Texas spread widely following rapid establishment, despite much later emergence (e.g. lineage 1: posterior mean TMRCA August 29, 95% CrI July 3 – September 25).



Fig. 4: Mobility-induced competition drives individual lineage spread.

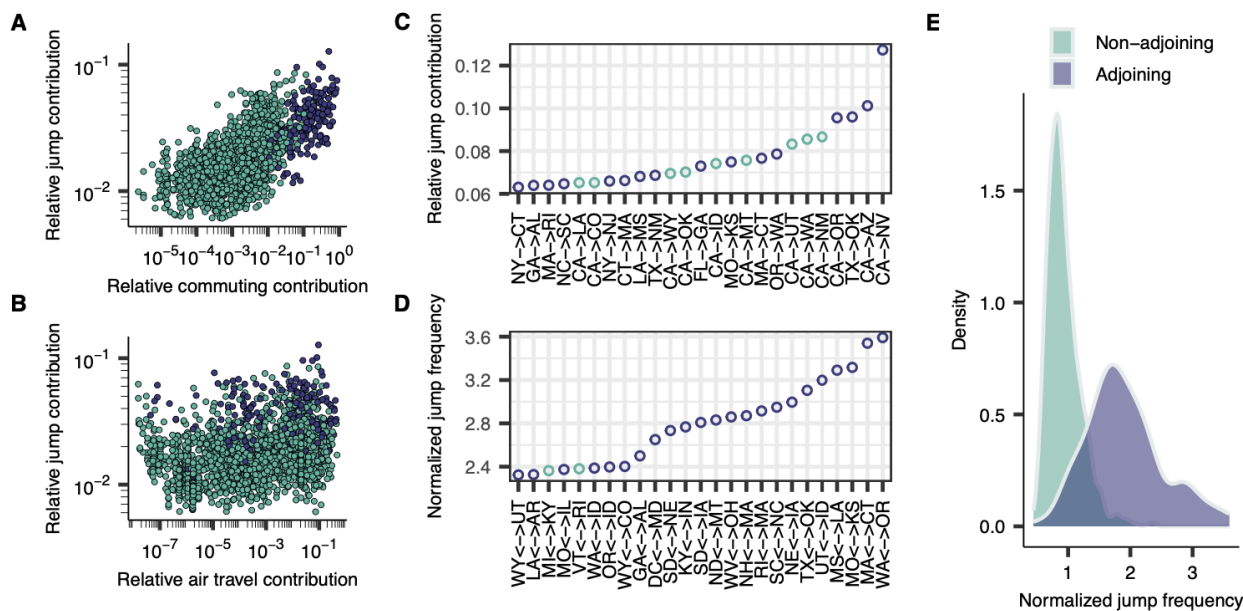
Phylogeny represents the 2019/2020 B/Victoria season, with the six largest lineages labeled in order of size. Top row of maps represents the reconstructed spread and distribution of each of the six largest lineages. Bottom row of maps represents the simulated spread and distribution of the six lineages, initialized in the lineages' respective onset state and onset week, simulated using a combination of air travel data and commuting data. Circle sizes are scaled as in Fig. 3.

Rates of reconstructed viral migration correlate with commuting and not air travel

Using mechanistic metapopulation simulations, the above results suggest that commuting flows are the primary mobility drivers of influenza virus spread. However, these reconstructions could only be performed for the seasons with relatively low lineage diversity, as the large number of co-circulating lineages in some seasons rendered sample counts too low for individual lineages to yield a reliable ground truth for reconstructions of spread. To confirm that commuting is the predominant drivers of viral spread when incorporating all lineages across all seasons in the analysis, we investigated if the same mobility processes were reflected in the genetic relationships between viruses in the lineage phylogenetic trees themselves. To do so, we leveraged phylogeographic analyses to compute the relative role of each state as a donor or recipient state of viral migration events for each other state. Here, the relative viral jump contribution $x \rightarrow y$ represents the

475 proportion of reconstructed migration events to and from state y that was accounted for
 476 by state x . Then, we correlated this metric of relative viral migration frequency with
 477 metrics of human mobility.

478
 479 The states with the greatest role as the source or destination of viral migration events
 480 to/from a given state tended to be the states that were most strongly connected through
 481 commuting flows to that state (Spearman $\rho = 0.63$, $P < 0.001$) (Fig. 5A). A correlation
 482 between relative jump contribution and air travel contribution was also present
 483 (Spearman $\rho = 0.32$, $P = <0.001$), but this correlation was weaker, with often a relatively
 484 high pairwise viral migration frequency even for states poorly linked through air travel
 485 (Fig. 5B). These results provide orthogonal support for the dominant role of commuting
 486 flows in driving seasonal influenza virus spread. We note that because we use a
 487 maximally uninformative phylogeographic model for viral migration, the model likely
 488 overestimates rates of spatially uncorrelated spread, but our conclusions are robust to
 489 such biases (see Materials and Methods).



491
 492 **Fig. 5: Phylogeographic analyses of mobility drivers.**

493 (A) Relationship between the relative contribution of each other state to a state’s inbound
 494 and outbound reconstructed viral migration events, and the other state’s relative role as a
 495 state’s commuting destination.

496 (B) Analogous to (A), for air travel data.

497 (C) Visualization of the 20 highest values of the relative jump contribution.

498 (D) Visualization of the 20 highest values for the normalized pairwise jump frequency.

499 (E) The distribution of normalized pairwise migration frequencies for pairs of adjoining
 500 and non-adjoining states.

501
 502 The highest values of the relative jump contribution $x \rightarrow y$ were found when state x was
 503 highly populous and state y was in close geographical proximity to state x . For example,
 504 the highest values across all pairs were found for CA→NV, CA→AZ, TX→OK,
 505 CA→OR, and CA→NM (Fig. 5C). This is expected under classical gravity-like spread
 506 where, for any given state, the highest connectivity is expected to be to states that are in
 507 close geographic proximity and highly populous. However, this pattern could be
 508 confounded by higher sample counts for the most populous states, as higher sample

509 counts for a deme in phylogeographic analyses will *a priori* be expected to lead to more
510 reconstructed migration events even in the absence of any spatial signal in the data. As
511 such, we also computed an alternative metric that accounts for this potential confounder.
512 Here, the normalized pairwise jump frequency $x \leftrightarrow y$ represents the proportion of
513 migration events to/from state y that is accounted for by state x , normalized relative to the
514 mean proportion of migration events that state x accounts for across all states. This
515 quantity is symmetric, i.e. $x \leftrightarrow y = y \leftrightarrow x$. The highest values were for adjacent states that
516 are strongly connected through commuting flows (highest: WA↔OR, MA↔CT,
517 MO↔KS, MS↔LA, UT↔ID (Fig. 5D), indicating that when accounting for effects of
518 population size and/or sampling, viral migration is strongly skewed toward short
519 distances. Consistent with this, the normalized pairwise migration frequency was
520 substantially greater for states that are adjacent than those that are non-adjacent (Fig. 5E).
521 These results provide further evidence for the important role of short-distance spatial
522 coupling in viral spread.

523 Discussion

524 Our analyses at the transmission lineage level reveal the structure of seasonal influenza
525 virus epidemics at a fine-grained resolution. Spread of individual lineages often occurred
526 in a clear spatiotemporal hierarchy, and the competitive co-circulation of different
527 lineages induced a strong spatial structure in seasonal influenza epidemics. The lineage
528 structure of epidemics cannot reliably be identified from epidemiological data alone, but
529 it is an essential component of seasonal influenza epidemiological dynamics. For
530 example inter-state patterns of spatial coupling at the transmission lineage level as
531 identified in this study differ substantially from patterns of similarity solely defined as
532 correlation of influenza-like illness in approximately the same time period (19).
533 Furthermore, the previously identified strong spatial coupling between the more
534 populous states from epidemic synchrony could be the result of concurrent processes of
535 epidemic establishment resulting from distinct seeding events, rather than the result of
536 hierarchical spread between different states (5, 26). Lineage structure is also key to
537 understanding seasonal influenza source-sink dynamics. Previous studies based on the
538 ILI data have posited that the South represents the dominant source of influenza virus
539 epidemics (4, 6). While our analyses reveal the frequent early establishment and national
540 success of lineages emerging in the South, this pattern was not consistent across seasons
541 and the lineage complexity of epidemics means that source-sink dynamics are highly
542 heterogeneous across seasons. Our inferences regarding source-sink dynamics also differ
543 from those in studies that implicitly assume that a single lineage generated all epidemic
544 activity in a given season (33).

545 Using a mechanistic epidemic model to reproduce lineage spread, we show that observed
546 dynamics of lineage spread are mostly driven by commuting flows, which generate the
547 network on which co-circulating lineages compete for disease-susceptible individuals. It
548 is striking that we could reproduce lineage spread dynamics using mechanistic
549 simulations when parameterizing mobility directly using commuter surveys. Commuting
550 data has previously been suggested to drive influenza viral spread based on analyses of
551 ILI data (4, 5), but this has not been shown mechanistically or validated against
552 phylogenetically supported instances of viral spread across (sub)types (4, 8, 23). While
553 we found a clear dominance of commuting over air travel when considering these metrics
554 in isolation, our results also suggested that air travel flows not captured in commuter
555 surveys could play a role in viral dissemination.

559
560 The competitive dynamics of individual lineages exhibit the characteristics of gravity-
561 like spread with localized, radial spread from less populous states, and strong long-range
562 connections allowing rapid cross-country spread from highly populous states. The
563 coupling induced by human mobility as reflected in the clear spatial hierarchies of
564 lineage spread provides an explanation why including spatial coupling has been found to
565 increase forecasting performance (18, 19). The often highly repeatable dynamics of
566 human mobility suggest a potential role for ensemble forecasts that integrate lineage-
567 specific epidemic dynamics with patterns of human mobility to predict epidemic make-
568 up. Upon local establishment of different lineages in different states, such simulations
569 could be used to forecast which lineages are likely to predominate where, but given the
570 stochastic dynamics of lineage establishment, forecasting efforts would also need to take
571 into account uncertainties arising from the potentially rapid spread of lineages that have
572 yet to establish. These forecasts could be especially valuable for public health planning if
573 antigenically distinct viruses establish transmission chains in different states, such as
574 observed in the 2018/2019 A/H3N2 season (31).

575
576 Early-season virologic surveillance data have been shown to give clues as to epidemic
577 subtype composition (20), but the importance of short-term lineage establishment
578 processes crucially suggests that the transmission chains corresponding to the earliest-
579 sampled viruses will often not propagate into periods of peak epidemic activity, limiting
580 the predictive utility of early-season genomic surveillance efforts. On the other hand, the
581 strong correspondence between lineage establishment timing and lineage size, where the
582 most dominant lineages are the ones that establish earliest, underscores the importance of
583 high-resolution information on where substantial levels of seasonal influenza virus
584 epidemic activity are occurring. Our study highlights the importance of nowcasting
585 efforts to identify the locations of epidemic establishment which, when combined with
586 high-resolution genomic surveillance in those areas, could be leveraged to generate more
587 robust predictions of lineage spread (19).

588
589 Our analyses have a number of limitations. The procedure used to classify viruses into
590 transmission lineages could introduce errors, but the strong spatial structures identified
591 lend credence to the clustering method used. Furthermore, we could only perform our
592 analyses at the state level owing to that being the level of spatial resolution in most virus
593 metadata, and analyses at other spatial scales may yield different results regarding modes
594 of virus spread (4, 34). Our analyses are limited by the relatively low evolutionary rate
595 and relatively limited sampling of influenza B viruses, complicating the accurate
596 delineation into transmission lineages. Mobility flows underlying the spread of influenza
597 B viruses are potentially different from those for influenza A viruses as a result of
598 differences in the age distribution of infection (2). However, the identification of
599 subtype-specific variation in dominant mobility flows was hampered by the substantial
600 variation in epidemic size among subtypes and seasons, which renders potential
601 differences in mobility flows difficult to disentangle from other sources of variation.
602 Nevertheless, our mechanistic simulations were able to recapitulate observed patterns of
603 spread using commuting data for influenza A and B viruses, suggesting similar
604 mechanisms drive the spread of both.

605
606 We found that many of the most successful transmission lineages emerged very shortly
607 before epidemic onset and established rapidly, sometimes sweeping to national
608 dominance despite substantial competition from other contemporaneous transmission

609 chains. The observed heterogeneity of transmission processes raises important questions
610 regarding the predictability of early-season seasonal influenza epidemiological dynamics
611 at multi-week time horizons, even in the presence of perfect data. The fact that seasonal
612 influenza forecasts rarely outperform models based on historical baseline activity at
613 timescales greater than a few weeks (22, 35) is likely tied to these heterogeneities. An
614 essential question remains what drives the timing and location of the highly explosive
615 epidemic sparks that can lead to rapid lineage expansion. It is striking that in some
616 seasons, the majority of peak-period circulation descended from a single ancestral virus
617 that existed when relatively substantial circulation was already ongoing. Epidemic
618 establishment processes are highly complex, likely influenced by many factors, including
619 but not limited to immune susceptibility (36–38), climate (11, 39, 40), spatial
620 organization (11), contact network structure (10), human behavior (41, 42), inter-subtype
621 competition (37, 43), and international (44) and domestic travel acting in concert. High-
622 resolution characterization of early-season epidemic dynamics at the transmission lineage
623 level among diverse geographical localities is likely necessary to disentangle the
624 contributions of these variables. Even if our results shed light on the potentially
625 predictable underlying drivers of viral migration, an understanding of all the above
626 factors will likely be necessary to probe the limits of seasonal influenza epidemic
627 predictability.
628

629
630
631
632
633
634
635
636
637
638
639
640
641
642
643
644
645
646
647
648
649
650
651
652
653
654
655
656
657
658
659
660
661
662
663
664
665
666
667
668
669
670
671
672
673
674
675
676
677
678

Materials & Methods

Data

We downloaded all influenza A and B virus sequences corresponding to the A/H3N2 or A/H1N1pdm09 subtypes and B/Victoria and B/Yamagata influenza B lineages, collected from humans in the United States between July 1st 2014 and July 1st 2023 from the GISAID (45) EpiFlu database. Throughout, we use the term ‘subtype’ to refer to the influenza A subtypes and influenza B lineages individually, to avoid confusion between transmission lineages and influenza B lineages. We limited the dataset to viruses with sequences available for all eight gene segments. Furthermore, we retained only virus sequences with the US Centers for Disease Control as submitting laboratory, to minimize the impact of targeted sequencing investigations that are potentially not representative and could bias the data, particularly the branching structure of phylogenies. This led to a full dataset consisting of 30,508 viruses (A/H3N2: 14,235, A/H1N1pdm09: 8,155, B/Yamagata: 3,543, B/Victoria: 4,584). We downloaded weekly proportions reporting for influenza-like illness by state and season for the same time period from the CDC FluView website (<https://www.cdc.gov/flu/weekly/fluviewinteractive.htm>). From this website, we also downloaded weekly counts of positive influenza A and B tests in clinical laboratories, and weekly counts of positive tests by influenza A subtype and influenza B lineage in public health laboratories, by state and season. For the 2014/2015 season, positive tests for clinical laboratories were stratified by (sub)type/lineage. We similarly downloaded the number of positive tests in public health laboratories at the national level. We downloaded data on commuting flows for 2016-2020 from the US Census Bureau (<https://www.census.gov/data/tables/2020/demo/metro-micro/commuting-flows-2020.html>). This data is stratified by origin and destination county. We downloaded data on air travel fluxes between states, stratified by origin and destination airport for the year 2017 from the US Bureau of Transportation Statistics (https://www.transtats.bts.gov/DL_SelectFields.aspx?gnoyr_VQ=GED&QO_fu146_anzr=).

Phylogenetic analyses

We aligned the sequences for each gene segment and subtype using MAFFT (46). We then clustered viruses, for each segment and subtype individually, into groups of highly related viruses using CD-HIT (47), with a clustering threshold of 99.5% nucleotide identity. Using a single representative virus for each cluster, we built a single tree for each subtype and segment individually using FastTree (48). We then fit a molecular clock to each tree using TempEst (49), and removed sequences belonging to CD-HIT-identified clusters for which the representative virus was classified as a molecular clock outlier from the dataset. This led to the removal of 40 viruses from the dataset. For each subtype, we then constructed a phylogenetic tree for each segment individually using all viruses for the entire period using IQTree (50) with a HKY (51) substitution model. We clustered the taxa in each of these trees by computing the largest groups of viruses where, for each taxon within a cluster, there was at least one other taxon in the group that saw a patristic distance to the former taxon that was smaller than a given distance threshold. We defined this distance threshold as the expected number of mutations over a two-year period given the estimated molecular clock rate for that segment and subtype/lineage; we used a more relaxed three-year period for the MP and NS segments for additional

679 lenience given their lower evolutionary rate. Using these cluster delineations, we
680 assigned each taxon a segment-specific cluster identity. Using the cluster identities for
681 each individual segment, we assigned each taxon a genome-wide cluster identity as the
682 combination of individual segment identities. These identities were defined for each
683 season individually, retaining the sequences from the 1st of January of the preceding
684 winter period up to the 1st of July of the following year. We concatenated the sequences
685 for all segments for viruses and constructed whole-genome phylogenetic trees for each of
686 the genome-wide cluster identities individually. Concatenating gene segments runs the
687 risk of introducing error due to potential reassortment events; we aimed to minimize this
688 risk by clustering all taxa into groups of similar viruses using the procedure described
689 above. We constructed phylogenies in IQTree (50) using a HKY (51) substitution model
690 using a segment-proportional model (52). Given these maximum-likelihood phylogenies,
691 we constructed temporally resolved trees using TreeTime (53) using a fixed clock rate
692 estimated using TempEst.

693 *Transmission lineage identification*

694
695 Using these time trees, we then sought to delineate the whole-genome phylogenetic trees
696 into individual transmission lineages. We defined transmission lineages as groups of taxa
697 on a phylogeny that plausibly descended from a common ancestor in the United States.
698 Given the exponential nature of influenza epidemics, we identified groups of highly
699 related viruses for which the tree structure follows the comb-like shape expected under
700 an exponential growth population dynamic process, where most coalescent events
701 happen close in time to the common ancestor. To do so, we used a modified version of
702 Phydely (54), a tool designed for the identification of transmission clusters on
703 phylogenies. We imposed the constraint that each transmission lineage was required to
704 exhibit the characteristic branching structure of exponential spread. Specifically, we
705 required that for each transmission lineage, a certain proportion p of all coalescent events
706 must occur within a particular period t of the putative lineage's root, with p and t
707 specified. Given the constraints, Phydely aims to cluster as many taxa as possible given
708 some constraints, formulating the problem as an integer linear programming (ILP)
709 problem. Here, every internal node in the phylogeny is a potential transmission cluster,
710 and the algorithm aims to cluster as many tips as possible, given the constraints.
711

712
713 If t is very high and p is very low the constraints imposed on the tree shape of a
714 transmission lineage are relatively less stringent. As a result, sensitivity is high for
715 purpose of clustering as many taxa as possible, but this might also result in erroneous
716 clustering if genetically similar viruses were independently seeded into the United States
717 and individually proliferated. On the other hand, a very stringent threshold (i.e. low t and
718 high p) will lead to high specificity, but might also lead to erroneous discarding of true
719 transmission lineages, as some true lineages will necessarily have a less comb-like
720 structure, for example if they emerged early in the season, outside of typical periods of
721 respiratory virus circulation, and spread at low levels before expanding when conditions
722 were favorable for large-scale transmission. In the main text, we chose $p = 0.10$ and $t =$
723 $1/12$, i.e. 10% of coalescent events in a lineage must occur in the first month after its
724 root. These values were chosen to balance sensitivity and specificity. We visualized the
725 clustered trees using the *ggtree* (55) package, presenting all transmission lineages in a
726 single tree. Because we clustered the trees into groups of similar viruses at the whole-
727 genome level before the identification of transmission lineages, we did not reconstruct
728 the ancestral relationships between all taxa. Hence, we only present the relationships

729 between taxa if they belonged to the same whole-genome cluster identity. Differences in
730 sampling among states could affect the delineations of viruses into clusters, principally
731 by affect the branching structure within putative clusters. We found a strong log-linear
732 relationship between a state's population size and its sequencing rate relative to its
733 population size (Pearson $r = -0.73$, $P < 0.001$), but some states had substantially greater
734 sampling rates than would be expected under the identified relationship given their
735 population size. To minimize effects of differences in sampling on cluster delineations,
736 we subsampled the taxa in each state, for each season-subtype pair, such that no state had
737 a number of sequences more than 0.5 log units greater than the regression-predicted
738 number given its population size.

740 To reconstruct the spatiotemporal spread dynamics of individual lineages, we integrated
741 the sampling date of each taxon with influenza-like illness and virological surveillance
742 data. For each season and state individually, we computed the influenza type-specific
743 disease signal by multiplying the proportion reporting influenza-like illness in each week
744 by the proportion of tests positive for influenza A and B separately, yielding a measure of
745 type-specific incidence. We then applied a 4253H, Twice smoother, implemented in the
746 *sleekts* R package, to smooth the epidemic curves. To extract transmission lineage-
747 specific epidemic curves, we fitted the sampling dates of taxa belonging to individual
748 transmission lineages to the reconstructed type-specific epidemic curves. For each state
749 and type (i.e. A or B) individually, we used a kernel density estimate given by a normal
750 distribution centered around each taxon's sampling date, with a two-week standard
751 deviation. We retained taxa that were not assigned to any transmission lineage as a
752 separate group. In each week, the relative incidence of a transmission lineage in that state
753 was given by the proportion of all kernel density estimate contributions in that week
754 corresponding to that lineage, multiplied by type-specific incidence.

756 Given each lineage's reconstructed epidemic dynamics in each state, we computed two
757 key state-level transmission lineage-specific summary statistics. 1) Lineage size,
758 computed by dividing the number of taxa sampled in each state belonging to a particular
759 by the total number of sequenced viruses in the state for that subtype, in the
760 corresponding season, i.e. ranging from 0 to 1; and 2) lineage establishment timing,
761 defined as the first week the lineage had accounted for at least 5% of total incidence in
762 that season (if at all), using the mapping of sequence sampling date to incidence data
763 described above. In some states, ILI and/or virologically confirmed data was absent for
764 all or some seasons; in these cases, we only computed the lineage size, and not the onset
765 week. Using these state-specific quantities, we computed nation-wide lineage size as the
766 sum of state-specific relative sizes divided by the number of states; hence, each state is
767 equal-weighted, irrespective of the state's population size or sample count. We also
768 computed the nation-wide time of lineage establishment as the first week of lineage
769 establishment in any state. For each state, in each subtype-season pair, we computed the
770 normalized Shannon entropy of the season's lineage composition, which equates to 1 if
771 each sampled virus corresponded to a different transmission lineage, and 0 if all sampled
772 viruses belonged to the same lineage. In the regression analyses for the determinants of
773 lineage size, we included only subtype-season pairs where the subtype accounted for
774 >10% of a season's total positive tests.

776 *Spread reconstruction*

729
730
731
732
733
734
735
736
737
738
739
740
741
742
743
744
745
746
747
748
749
750
751
752
753
754
755
756
757
758
759
760
761
762
763
764
765
766
767
768
769
770
771
772
773
774
775
776
777

778 To characterize the similarity of lineage compositions across all pairs of states, we
779 computed the median Bray-Curtis similarity for all pairs of states. We sampled 20
780 clustered viruses from each state for each season across all (sub)types (or retained all if
781 fewer than 20 sequences were available) and computed the Bray-Curtis similarity of the
782 transmission lineages corresponding to the sampled viruses using the *vegdist* command
783 in the *vegan* (56) R package. We performed this procedure 50 times, retaining the mean
784 value of each pair of states' similarity across all replicates. All analyses were performed
785 for the seasons from 2014/2015 to 2019/2020 and 2022/2023, omitting the 2021/2022
786 season due to its aberrant epidemic dynamics following the COVID-19 pandemic; this
787 season saw substantial levels of circulation during the summer period, complicating the
788 delineation of lineages into individual seasons. We retained only states with at least 10
789 sequences in all seasons, leaving a set of 42 states.

790
791 We performed hierarchical clustering on the similarity matrix across all seasons/subtypes
792 using the *hclust* R function, using complete linkage clustering. We performed isometric
793 multi-dimensional scaling using the *isoMDS* function in the *MASS* R package. To
794 compute the correlation states between compositional similarity and centroid distance,
795 we correlated the similarity matrix with states' centroid distances using the *mantel*
796 command in the *vegan* package. We performed these analyses at the individual season-
797 subtype pair level in the same fashion, sampling 10 viruses from the set of clustered taxa
798 sampled in that season for that subtype and computing the Bray-Curtis similarity as
799 described above. Here, we retained only season-subtype pairs that saw at least 40 states
800 with at least 10 clustered viruses.

801 *Source-sink phylogeographic inference*

802
803
804 For the analyses of source-sink dynamics, we performed phylogeographic analyses in
805 BEAST (30) for all transmission lineages that accounted for at least 0.5% of all
806 sequenced viruses in a given season across all subtypes. We performed these analyses at
807 the level of Health and Human Services (HHS) region, to allow for substantial spatial
808 granularity while also having sufficient sequence counts per spatial unit. We used
809 Thorney BEAST, implemented in BEAST (30) v2.3.31, to estimate a distribution of
810 time-resolved phylogenies for each individual lineage, marginalizing over bifurcating
811 topologies consistent with the potentially multifurcating input tree. We used divergence
812 trees estimated in IQTREE, as explained above, as input trees, extracting the subtrees
813 that corresponded to each transmission lineage. We furnished all transmission lineages
814 with fewer than 50 taxa with an exponential growth coalescent prior, and a Skygrid (57)
815 coalescent prior for all transmission lineages with at least 50 taxa. We estimated a single
816 clock rate for each season-subtype pair. For each season-subtype pair, we ran a single
817 MCMC chain for 500 million iterations, sampling lineage trees every 5 million states.
818 We assessed convergence using Tracer (58), and generated a set of 90 posterior trees for
819 each transmission lineage using TreeAnnotator (<https://beast.community/treannotator>),
820 removing the first 10% as burn-in.

821
822 We performed discrete trait phylogeographic inference (59) using the posterior lineage
823 trees. We used a CTMC model for migration where we assumed equal rates of migration
824 between all regions. We used this model as many lineages had relatively few sequences,
825 prohibiting the reliable estimation of pairwise region-to-region migration rates.
826 Furthermore, these rates could not realistically be shared across transmission lineages as
827 dynamics of migration vary substantially from lineage to lineage depending on the

828 location of emergence and the landscape of lineage competition, and are likely highly
829 temporally inhomogeneous, with dominance of the origin state early on but more
830 spatially diffuse spread later. We ran these analyses for 100 million iterations, sampling
831 every million, and removed the first 10% for each lineage as burn-in. We leveraged
832 stochastic mapping (60) to identify migration events on the posterior phylogenies. Using
833 these reconstructed migration events, we identified the likely origin of each lineage in
834 each sample as the HHS region that was the source for most of the first 10 migration
835 events in each lineage. We used this definition for the lineage origin rather than simply
836 the reconstructed root region as we were primarily interested in the rapid expansion of
837 lineages, and the root could be affected by the inclusion of unrelated singleton viruses in
838 the analysis that did not contribute to lineage expansion. Reassuringly, we found that for
839 most transmission lineages, lineage source posterior probabilities were generally focused
840 on a small number of HHS regions.

841
842 Using the lineage origin posterior distributions, we then computed state-specific origin
843 profiles, which represent the posterior proportion of sampled viruses in a focal state that
844 belonged to lineages that were reconstructed to have originally expanded in each HHS
845 region. Here, we aggregated across all subtypes and seasons, weighting each lineage
846 according to the total proportion of circulation it accounted in the corresponding season
847 in the focal state, across all subtypes. To investigate spatial structure in these source
848 profiles, we correlated the Euclidean distance of these profiles between states with the
849 centroid distance between the states using a Mantel test. Because we expected higher
850 similarity between states in the same HHS region because they represent a single group
851 in the phylogeographic reconstructions, we only performed this analysis for states that
852 were not in the same HHS region. For any given state, we only included those seasons
853 where that state had at least 10 sampled viruses when computing the source profiles, to
854 prevent stochastic sampling effects from biasing results when sequence counts were low
855 in a given season.

856
857 Phylogeographic reconstructions are prone to bias resulting from differences in sampling
858 rates among the geographical groupings. To assess the sensitivity of our results with
859 respect to these biases, we used two different sampling strategies. For our first sampling
860 strategy, we used a sampling strategy where sequences from states that had a sequence
861 count that was greater than expected from the regression line relating sequencing rate to
862 population size were subsampled to the sequence count predicted from the regression line
863 given its population size. This subsampling strategy was akin to the subsampling strategy
864 used for the cluster delineations described above, but more stringent. Hence, the sample
865 count for each HHS region was roughly proportional to the region's population size. For
866 the second sampling strategy, we ensured that the number of taxa included for each HHS
867 region was approximately uniform, irrespective of the HHS region's population size. For
868 each season-subtype combination, we computed the sequence count as the 25th quantile
869 of the number of sequences in each HHS region in the population-proportional
870 subsampling scheme used above. For regions with more sequences than this value,
871 sequences were randomly subsampled. Because the results of the inferences are subject
872 to variation due to the sampling strategy used, we mainly reported among-state
873 differences for any given sampling strategy, and de-emphasized the absolute proportions
874 estimated using the different models. For the same reason, we reported the likely origins
875 of the largest lineages averaged across both sampling strategies. Nevertheless, the strong
876 correlation between two sampling strategies suggests that sampling effects do not
877 dominate the results.

878
879 To correlate mobility with rates of inter-state viral migration as reflected in the lineage
880 phylogenies (Fig. 5), we performed Bayesian phylogeographic analyses analogous to the
881 source-sink analyses above. We used the same procedure to perform phylogeographic
882 reconstructions at the state level instead of the HHS region level, using the population-
883 weighted subsampling strategy where sequences from states with higher sequencing rate
884 than expected for their population were subsampled to the regression-predicted
885 sequencing rate. We then reconstructed Markov jumps across all posterior trees for all
886 transmission lineages. Then, for each pair of states x and y , we computed the relative
887 jump contribution $x \rightarrow y$ as the proportion of migration events to and from state y that was
888 accounted for by state x . We analogously computed the proportion of travelers from state
889 y that had state x as destination for the air travel and commuting data and correlated these
890 quantities with the relative jump contributions as estimated from the phylogenies. Here,
891 we added a pseudocount for pairs of states with zero commuters or air travelers. We also
892 computed the normalized relative jump frequency $x \leftrightarrow y$, which represents the proportion
893 of migration events to/from state y that is accounted for by state x , normalized relative to
894 the mean proportion of migration events that state x accounts for across all states. These
895 values are highly symmetric (Pearson $r = 0.997$), and hence we symmetrized to subsume
896 pairs of states. By comparing the jump frequency between states relative to the states'
897 mean, this metric is not prone to potential biases resulting from differences in sampling
898 across states. However, a limitation of this metric is that only allows for ascertainment of
899 the effect of distance and not of characteristics that are intrinsic to a single location, such
900 as population size.

901
902 Because we used an equal-rates model for viral migration, the values of the relative jump
903 contributions will likely overestimate rates of viral migration between spatially distant
904 localities that are not well-connected through mobility. This is an inherent limitation of
905 the model used. However, due to the complex migration dynamics that are likely highly
906 time-inhomogeneous and differ substantially across lineages (as described above),
907 migration patterns can likely not be captured by a single rate across all lineages and
908 points in time, nor can time-inhomogeneous rates reliably be estimated or parameterized.
909 These limitations also apply to alternative models such as a GLM formulation (44).
910 Correlating reconstructed viral migration rates with metrics of mobility in *post hoc*
911 analyses rather than including these metrics as covariates in the migration rate
912 parameterizations affords certainty that the identified relationship between viral
913 migration and human mobility is not a statistical artefact. The fact that we established a
914 strong correlation between commuting rates and viral migration rates provides support
915 for the use of the simplified model.

916 *Metapopulation model*

917
918 With the aim of reproducing the observed spread of co-circulating lineages, particularly
919 the lineages' distribution among states, we used a mechanistic epidemic model that
920 simulates the inter-state spread of co-circulating SIR-type pathogens with perfect cross-
921 immunity that compete for disease-susceptible individuals. To limit the computational
922 burden, we used a deterministic model that stratifies each epidemiological state into three
923 further compartments for individuals remaining in their home state and for those visiting
924 another state by commuting and air travel respectively. The model dynamics are then as
925 follows:
926
927

928
929
930
931
932
933
934
935
936
937
938
939
940
941
942
943
944
945
946
947
948
949
950
951
952
953
954
955
956
957
958
959
960
961
962
963
964
965
966
967
968
969
970
971

$$\begin{aligned} \frac{dS_{ijm}}{dt} &= -\beta I_{ijm} \frac{\sum_{j,m} S_{ijm} + S_{ii}}{\sum_{j,m} N_{ijm} + N_{ii}} + S_{jj} l_{ijm} - S_{ijm} r \\ \frac{dS_{ii}}{dt} &= -\beta I_{ii} \frac{\sum_{j,m} S_{ijm} + S_{ii}}{\sum_{j,m} N_{ijm} + N_{ii}} - \sum_{j,m} S_{ii} l_{jim} + \sum_{j,m} S_{jim} r \\ \frac{dI_{ijm}}{dt} &= \beta I_{ijm} \frac{\sum_{j,m} S_{ijm} + S_{ii}}{\sum_{j,m} N_{ijm} + N_{ii}} - \gamma I_{ijm} + I_{jj} l_{ijm} - I_{ijm} r \\ \frac{dI_{ii}}{dt} &= \beta I_{ii} \frac{\sum_{j,m} S_{ijm} + S_{ii}}{\sum_{j,m} N_{ijm} + N_{ii}} - \gamma I_{ii} - \sum_{j,m} I_{ii} l_{jim} + \sum_{j,m} I_{jim} r \end{aligned}$$

Here, S_{ijm} and I_{ijm} represent the number of susceptible and infected individuals, respectively, originating from state j that are currently in state i for mobility modality m . m can represent either commuting or air travel. Analogously, S_{jj} and I_{jj} represent the number of susceptible and infected individuals, respectively that are at home in state j . Matrix l represent the outward travel rates for each mobility modality and r represents the return rate. We assume $r = 1 \text{ day}^{-1}$, $\gamma = 0.25$, and $R_0 = 1.35$. For state-to-state air travel rates, we computed the rate of air travel between states x and y as the total number of passengers in 2016 between airports located in state x and state y , and symmetrized the counts by computing the mean of the two counts. We then computed a daily rate from x to y by as the states' symmetrized trip count divided by 365 and the population size of state x . We computed the number of commuters between each pair of states by aggregating across origin and destination counties in each state. We analogously symmetrized these counts (though they are highly symmetric, $r = 0.9998$) and computed the daily commuting rate $x \rightarrow y$ as the number of symmetrized commuters between the two states divided by the population size of state x . For the simulations that used a combination of air travel and commuting flows, the rate between each pair of states was defined as the maximum of the pairwise commuting and air travel rates, to account for the possibility that some of the commuting flows are accounted for by the air travel data. The model was implemented in C++, interfacing with R using Rcpp (61).

Using the metapopulation model, we investigated if we could recapitulate the distribution of lineages across the country, given the timing and location of each lineage's onset, under the model of competition between lineages for susceptible individuals on the mobility network. For the set of lineages that were simulated, we simulated the epidemic progression forward in time, initializing each lineage in its reconstructed first week of establishment (see above), in its likely onset state. As the lineage's onset week, we took the first week of establishment of the lineage in any state, rather than in the onset state, to account for situations where incidence data was absent for the likely onset state. However, we allowed each lineage's onset week to vary to up to two weeks after or two weeks before its estimated data, to account for situations where the index state did not have incidence data available, and to account for error arising from the estimation of lineage-specific establishment timings with relatively noisy data. Lineages were initialized with an infected population of 1×10^{-5} times the index state's population size. Analogous to the ground truth reconstructions, we computed the size of each lineage in the reconstructions as the proportion of infections across simulated lineages in a state that was attributable to a particular lineage. Similarly, we computed the week of establishment as the first week a lineage had caused $>5\%$ of total infections across simulated lineages in the full simulations. Because the simulations only included a limited set of lineages, we visualized the simulations by scaling the circles for each state

972 such that the total size of the circles for the simulated lineages was proportional to the
973 total proportion of sequences in each state that was accounted for by the simulated
974 lineages.
975
976

References

1. T. Bedford, S. Cobey, P. Beerli, M. Pascual, Global Migration Dynamics Underlie Evolution and Persistence of Human Influenza A (H3N2). *PLOS Pathog.* **6**, e1000918- (2010).
2. T. Bedford, S. Riley, I. G. Barr, S. Broor, M. Chadha, N. J. Cox, R. S. Daniels, C. P. Gunasekaran, A. C. Hurt, A. Kelso, A. Klimov, N. S. Lewis, X. Li, J. W. McCauley, T. Odagiri, V. Potdar, A. Rambaut, Y. Shu, E. Skepner, D. J. Smith, M. A. Suchard, M. Tashiro, D. Wang, X. Xu, P. Lemey, C. A. Russell, Global circulation patterns of seasonal influenza viruses vary with antigenic drift. *Nature* **523**, 217–220 (2015).
3. R. C. A, J. T. C, B. I. G, C. N. J, G. R. J, G. Vicky, G. I. D, H. A. W, H. A. J, H. A. C, de J. J. C, K. Anne, K. A. I, K. Tsutomu, K. Naomi, L. A. S, L. Y. P, M. Ana, O. Masatsugu, O. Takato, O. A. D. M. E, R. G. F, S. M. W, S. Eugene, S. Klaus, T. Masato, F. R. A. M, S. D. J, The Global Circulation of Seasonal Influenza A (H3N2) Viruses. *Science (80-.)*. **320**, 340–346 (2008).
4. V. Charu, S. Zeger, J. Gog, O. N. Bjørnstad, S. Kissler, L. Simonsen, B. T. Grenfell, C. Viboud, Human mobility and the spatial transmission of influenza in the United States. *PLOS Comput. Biol.* **13**, e1005382- (2017).
5. V. Cécile, B. O. N, S. D. L, S. Lone, M. M. A, G. B. T, Synchrony, Waves, and Spatial Hierarchies in the Spread of Influenza. *Science (80-.)*. **312**, 447–451 (2006).
6. I. Chattopadhyay, E. Kiciman, J. W. Elliott, J. L. Shaman, A. Rzhetsky, Conjunction of factors triggering waves of seasonal influenza. *Elife* **7**, e30756 (2018).
7. S. Pei, S. Kandula, W. Yang, J. Shaman, Forecasting the spatial transmission of influenza in the United States. *Proc. Natl. Acad. Sci.* **115**, 2752 (2018).
8. B. A. Bozick, L. A. Real, The Role of Human Transportation Networks in Mediating the Genetic Structure of Seasonal Influenza in the United States. *PLOS Pathog.* **11**, e1004898- (2015).
9. D. Balcan, V. Colizza, B. Gonçalves, H. Hu, J. J. Ramasco, A. Vespignani, Multiscale mobility networks and the spatial spreading of infectious diseases. *Proc. Natl. Acad. Sci.* **106**, 21484 (2009).
10. S. Cauchemez, A.-J. Valleron, P.-Y. Boëlle, A. Flahault, N. M. Ferguson, Estimating the impact of school closure on influenza transmission from Sentinel data. *Nature* **452**, 750–754 (2008).
11. D. B. D, K. Stephen, G. J. R, V. Cecile, B. O. N, M. C. J. E, G. B. T, Urbanization and humidity shape the intensity of influenza epidemics in U.S. cities. *Science (80-.)*. **362**, 75–79 (2018).
12. W. Yang, M. Lipsitch, J. Shaman, Inference of seasonal and pandemic influenza transmission dynamics. *Proc. Natl. Acad. Sci.* **112**, 2723 (2015).
13. S. P. J. de Jong, Z. C. Felix Garza, J. C. Gibson, S. van Leeuwen, R. P. de Vries, G.-J. Boons, M. van Hoesel, K. de Haan, L. E. van Groenigen, K. D. Hulme, H. D. G. van Willigen, E. Wynberg, G. J. de Bree, A. Matser, M. Bakker, L. van der Hoek, M. Prins, N. A. Kootstra, D. Eggink, B. E. Nichols, A. X. Han, M. D. de Jong, C. A. Russell, Determinants of epidemic size and the impacts of lulls in seasonal influenza virus circulation. *Nat. Commun.* **15**, 591 (2024).
14. N. G. Reich, L. C. Brooks, S. J. Fox, S. Kandula, C. J. McGowan, E. Moore, D. Osthus, E. L. Ray, A. Tushar, T. K. Yamana, M. Biggerstaff, M. A. Johansson, R. Rosenfeld, J. Shaman, A collaborative multiyear, multimodel assessment of seasonal influenza forecasting in the United States. *Proc. Natl. Acad. Sci.* **116**, 3146 (2019).
15. J. Shaman, A. Karspeck, Forecasting seasonal outbreaks of influenza. *Proc. Natl. Acad. Sci.* **109**, 20425 (2012).

- 1027 16. M. Biggerstaff, M. Johansson, D. Alper, L. C. Brooks, P. Chakraborty, D. C. Farrow, S.
1028 Hyun, S. Kandula, C. McGowan, N. Ramakrishnan, R. Rosenfeld, J. Shaman, R.
1029 Tibshirani, R. J. Tibshirani, A. Vespignani, W. Yang, Q. Zhang, C. Reed, Results from
1030 the second year of a collaborative effort to forecast influenza seasons in the United States.
1031 *Epidemics* **24**, 26–33 (2018).
- 1032 17. M. Ben-Nun, P. Riley, J. Turtle, D. P. Bacon, S. Riley, Forecasting national and regional
1033 influenza-like illness for the USA. *PLOS Comput. Biol.* **15**, e1007013- (2019).
- 1034 18. A. E. L, N. A. T, V. Cecile, S. Mauricio, Toward the use of neural networks for influenza
1035 prediction at multiple spatial resolutions. *Sci. Adv.* **7**, eabb1237 (2022).
- 1036 19. F. S. Lu, M. W. Hattab, C. L. Clemente, M. Biggerstaff, M. Santillana, Improved state-
1037 level influenza nowcasting in the United States leveraging Internet-based data and
1038 network approaches. *Nat. Commun.* **10**, 147 (2019).
- 1039 20. E. Goldstein, S. Cobey, S. Takahashi, J. C. Miller, M. Lipsitch, Predicting the Epidemic
1040 Sizes of Influenza A/H1N1, A/H3N2, and B: A Statistical Method. *PLOS Med.* **8**,
1041 e1001051- (2011).
- 1042 21. D. Osthus, K. R. Moran, Multiscale influenza forecasting. *Nat. Commun.* **12**, 2991 (2021).
- 1043 22. C. Viboud, A. Vespignani, The future of influenza forecasts. *Proc. Natl. Acad. Sci.* **116**,
1044 2802–2804 (2019).
- 1045 23. C. Viboud, M. I. Nelson, Y. Tan, E. C. Holmes, Contrasting the epidemiological and
1046 evolutionary dynamics of influenza spatial transmission. *Philos. Trans. R. Soc. B Biol.*
1047 *Sci.* **368**, 20120199 (2013).
- 1048 24. M. I. Nelson, L. Simonsen, C. Viboud, M. A. Miller, J. Taylor, K. S. George, S. B.
1049 Griesemer, E. Ghedin, N. A. Sengamalay, D. J. Spiro, I. Volkov, B. T. Grenfell, D. J.
1050 Lipman, J. K. Taubenberger, E. C. Holmes, Stochastic Processes Are Key Determinants
1051 of Short-Term Evolution in Influenza A Virus. *PLOS Pathog.* **2**, e125- (2006).
- 1052 25. M. I. Nelson, L. Edelman, D. J. Spiro, A. R. Boyne, J. Bera, R. Halpin, E. Ghedin, M. A.
1053 Miller, L. Simonsen, C. Viboud, E. C. Holmes, Molecular Epidemiology of A/H3N2 and
1054 A/H1N1 Influenza Virus during a Single Epidemic Season in the United States. *PLOS*
1055 *Pathog.* **4**, e1000133 (2008).
- 1056 26. P. Crépey, M. Barthélemy, Detecting Robust Patterns in the Spread of Epidemics: A Case
1057 Study of Influenza in the United States and France. *Am. J. Epidemiol.* **166**, 1244–1251
1058 (2007).
- 1059 27. M. N. F, W. Cassia, F. C. D, R. Pavitra, L. Jover, M. L. H, P. Benjamin, R. Matthew, R.
1060 Erica, X. Hong, S. Lasata, A. Amin, R. V. M, L. N. A. P, H. Meei-Li, G. Romesh, M.
1061 Geoff, H. Brian, D. Philip, A. Amanda, B. Elisabeth, H. P. D, F. Kairsten, I. Misja, L.
1062 Kirsten, S. T. R, T. Melissa, W. C. R, B. Michael, E. J. A, F. Michael, L. B. R, R. M. J, T.
1063 Matthew, D. J. S, S. L. M, C. H. Y, S. Jay, J. K. R, L. Scott, G. A. L, N. D. A, B. Trevor,
1064 Viral genomes reveal patterns of the SARS-CoV-2 outbreak in Washington State. *Sci.*
1065 *Transl. Med.* **13**, eabf0202 (2021).
- 1066 28. D. Vijaykrishna, E. C. Holmes, U. Joseph, M. Fourment, Y. C. F. Su, R. Halpin, R. T. C.
1067 Lee, Y.-M. Deng, V. Gunalan, X. Lin, T. B. Stockwell, N. B. Fedorova, B. Zhou, N.
1068 Spirason, D. Kühnert, V. Bošková, T. Stadler, A.-M. Costa, D. E. Dwyer, Q. S. Huang, L.
1069 C. Jennings, W. Rawlinson, S. G. Sullivan, A. C. Hurt, S. Maurer-Stroh, D. E.
1070 Wentworth, G. J. D. Smith, I. G. Barr, The contrasting phylodynamics of human influenza
1071 B viruses. *Elife* **4**, e05055 (2015).
- 1072 29. B. I. Potter, R. Kondor, J. Hadfield, J. Huddleston, J. Barnes, T. Rowe, L. Guo, X. Xu, R.
1073 A. Neher, T. Bedford, D. E. Wentworth, Evolution and rapid spread of a reassortant
1074 A(H3N2) virus that predominated the 2017–2018 influenza season. *Virus Evol.* **5**, vez046
1075 (2019).
- 1076 30. M. A. Suchard, P. Lemey, G. Baele, D. L. Ayres, A. J. Drummond, A. Rambaut, Bayesian

- 1077 phylogenetic and phylodynamic data integration using BEAST 1.10. *Virus Evol.* **4**,
1078 vey016 (2018).
- 1079 31. B. Flannery, R. J. G. Kondor, J. R. Chung, M. Gaglani, M. Reis, R. K. Zimmerman, M. P.
1080 Nowalk, M. L. Jackson, L. A. Jackson, A. S. Monto, E. T. Martin, E. A. Belongia, H. Q.
1081 McLean, S. S. Kim, L. Blanton, K. Kniss, A. P. Budd, L. Brammer, T. J. Stark, J. R.
1082 Barnes, D. E. Wentworth, A. M. Fry, M. Patel, Spread of Antigenically Drifted Influenza
1083 A(H3N2) Viruses and Vaccine Effectiveness in the United States During the 2018–2019
1084 Season. *J. Infect. Dis.* **221**, 8–15 (2020).
- 1085 32. R. K. Borchering, C. E. Gunning, D. V Gokhale, K. B. Weedop, A. Saeidpour, T. S. Brett,
1086 P. Rohani, Anomalous influenza seasonality in the United States and the emergence of
1087 novel influenza B viruses. *Proc. Natl. Acad. Sci.* **118**, e2012327118 (2021).
- 1088 33. D. Magee, M. A. Suchard, M. Scotch, Bayesian phylogeography of influenza A/H3N2 for
1089 the 2014–15 season in the United States using three frameworks of ancestral state
1090 reconstruction. *PLOS Comput. Biol.* **13**, e1005389 (2017).
- 1091 34. S. Venkatramanan, A. Sadilek, A. Fadikar, C. L. Barrett, M. Biggerstaff, J. Chen, X.
1092 Dotiwalla, P. Eastham, B. Gipson, D. Higdon, O. Kucuktunc, A. Lieber, B. L. Lewis, Z.
1093 Reynolds, A. K. Vullikanti, L. Wang, M. Marathe, Forecasting influenza activity using
1094 machine-learned mobility map. *Nat. Commun.* **12**, 726 (2021).
- 1095 35. S. M. Mathis, A. E. Webber, T. M. León, E. L. Murray, M. Sun, L. A. White, L. C.
1096 Brooks, A. Green, A. J. Hu, R. Rosenfeld, D. Shemetov, R. J. Tibshirani, D. J. McDonald,
1097 S. Kandula, S. Pei, R. Yaari, T. K. Yamana, J. Shaman, P. Agarwal, S. Balusu, G.
1098 Gururajan, H. Kamarthi, B. A. Prakash, R. Raman, Z. Zhao, A. Rodríguez, A. Meiyappan,
1099 S. Omar, P. Baccam, H. L. Gurung, B. T. Suchoski, S. A. Stage, M. Ajelli, A. G.
1100 Kummer, M. Litvinova, P. C. Ventura, S. Wadsworth, J. Niemi, E. Carcelen, A. L. Hill, S.
1101 L. Loo, C. D. McKee, K. Sato, C. Smith, S. Truelove, S. Jung, J. C. Lemaitre, J. Lessler,
1102 T. McAndrew, W. Ye, N. Bosse, W. S. Hlavacek, Y. T. Lin, A. Mallela, G. C. Gibson, Y.
1103 Chen, S. M. Lamm, J. Lee, R. G. Posner, A. C. Perofsky, C. Viboud, L. Clemente, F. Lu,
1104 A. G. Meyer, M. Santillana, M. Chinazzi, J. T. Davis, K. Mu, A. Pastore y Piontti, A.
1105 Vespignani, X. Xiong, M. Ben-Nun, P. Riley, J. Turtle, C. Hulme-Lowe, S. Jessa, V. P.
1106 Nagraj, S. D. Turner, D. Williams, A. Basu, J. M. Drake, S. J. Fox, E. Suez, M. G.
1107 Cojocar, E. W. Thommes, E. Y. Cramer, A. Gerding, A. Stark, E. L. Ray, N. G. Reich,
1108 L. Shandross, N. Wattanachit, Y. Wang, M. W. Zorn, M. Al Aawar, A. Srivastava, L. A.
1109 Meyers, A. Adiga, B. Hurt, G. Kaur, B. L. Lewis, M. Marathe, S. Venkatramanan, P.
1110 Butler, A. Farabow, N. Ramakrishnan, N. Muralidhar, C. Reed, M. Biggerstaff, R. K.
1111 Borchering, Title evaluation of FluSight influenza forecasting in the 2021–22 and 2022–
1112 23 seasons with a new target laboratory-confirmed influenza hospitalizations. *Nat.*
1113 *Commun.* **15**, 6289 (2024).
- 1114 36. S. Gouma, K. Kim, M. E. Weirick, M. E. Gumina, A. Branche, D. J. Topham, E. T.
1115 Martin, A. S. Monto, S. Cobey, S. E. Hensley, Middle-aged individuals may be in a
1116 perpetual state of H3N2 influenza virus susceptibility. *Nat. Commun.* **11**, 4566 (2020).
- 1117 37. A. C. Perofsky, J. Huddleston, C. Hansen, J. R. Barnes, T. Rowe, X. Xu, R. Kondor, D. E.
1118 Wentworth, N. Lewis, L. Whittaker, B. Ermetal, R. Harvey, M. Galiano, R. S. Daniels, J.
1119 W. McCauley, S. Fujisaki, K. Nakamura, N. Kishida, S. Watanabe, H. Hasegawa, S. G.
1120 Sullivan, I. G. Barr, K. Subbarao, F. Krammer, T. Bedford, C. Viboud, Antigenic drift and
1121 subtype interference shape A(H3N2) epidemic dynamics in the United States. Cold Spring
1122 Harbor Laboratory (2023). <https://doi.org/10.1101/2023.10.02.23296453>.
- 1123 38. T. Bedford, M. A. Suchard, P. Lemey, G. Dudas, V. Gregory, A. J. Hay, J. W. McCauley,
1124 C. A. Russell, D. J. Smith, A. Rambaut, Integrating influenza antigenic dynamics with
1125 molecular evolution. *Elife* **3**, e01914 (2014).
- 1126 39. J. Shaman, V. E. Pitzer, C. Viboud, B. T. Grenfell, M. Lipsitch, Absolute Humidity and

- 1127 the Seasonal Onset of Influenza in the Continental United States. *PLOS Biol.* **8**,
1128 e1000316- (2010).
- 1129 40. J. D. Tamerius, J. Shaman, W. J. Alonso, K. Bloom-Feshbach, C. K. Uejio, A. Comrie, C.
1130 Viboud, Environmental Predictors of Seasonal Influenza Epidemics across Temperate and
1131 Tropical Climates. *PLOS Pathog.* **9**, e1003194- (2013).
- 1132 41. Q. S. Huang, T. Wood, L. Jelley, T. Jennings, S. Jefferies, K. Daniells, A. Nesdale, T.
1133 Dowell, N. Turner, P. Campbell-Stokes, M. Balm, H. C. Dobinson, C. C. Grant, S. James,
1134 N. Aminisani, J. Ralston, W. Gunn, J. Bocacao, J. Danielewicz, T. Moncrieff, A. McNeill,
1135 L. Lopez, B. Waite, T. Kiedrzyński, H. Schrader, R. Gray, K. Cook, D. Currin, C.
1136 Engelbrecht, W. Tapurau, L. Emmerton, M. Martin, M. G. Baker, S. Taylor, A.
1137 Trenholme, C. Wong, S. Lawrence, C. McArthur, A. Stanley, S. Roberts, F. Rahnama, J.
1138 Bennett, C. Mansell, M. Dilcher, A. Werno, J. Grant, A. van der Linden, B. Youngblood,
1139 P. G. Thomas, R. J. Webby, Npi. Consortium, Impact of the COVID-19
1140 nonpharmaceutical interventions on influenza and other respiratory viral infections in
1141 New Zealand. *Nat. Commun.* **12**, 1001 (2021).
- 1142 42. A. C. Perofsky, C. L. Hansen, R. Burstein, S. Boyle, R. Prentice, C. Marshall, D.
1143 Reinhart, B. Capodanno, M. Truong, K. Schwabe-Fry, K. Kuchta, B. Pfau, Z. Acker, J.
1144 Lee, T. R. Sibley, E. McDermot, L. Rodriguez-Salas, J. Stone, L. Gamboa, P. D. Han, A.
1145 Adler, A. Waghmare, M. L. Jackson, M. Famulare, J. Shendure, T. Bedford, H. Y. Chu, J.
1146 A. Englund, L. M. Starita, C. Viboud, Impacts of human mobility on the citywide
1147 transmission dynamics of 18 respiratory viruses in pre- and post-COVID-19 pandemic
1148 years. *Nat. Commun.* **15**, 4164 (2024).
- 1149 43. E. K. S. Lam, D. H. Morris, A. C. Hurt, I. G. Barr, C. A. Russell, The impact of climate
1150 and antigenic evolution on seasonal influenza virus epidemics in Australia. *Nat. Commun.*
1151 **11**, 2741 (2020).
- 1152 44. P. Lemey, A. Rambaut, T. Bedford, N. Faria, F. Bielejec, G. Baele, C. A. Russell, D. J.
1153 Smith, O. G. Pybus, D. Brockmann, M. A. Suchard, Unifying Viral Genetics and Human
1154 Transportation Data to Predict the Global Transmission Dynamics of Human Influenza
1155 H3N2. *PLOS Pathog.* **10**, e1003932- (2014).
- 1156 45. Y. Shu, J. McCauley, GISAID: Global initiative on sharing all influenza data - from
1157 vision to reality. (2017). <https://doi.org/10.2807/1560-7917.ES.2017.22.13.30494>.
- 1158 46. K. Katoh, D. M. Standley, MAFFT Multiple Sequence Alignment Software Version 7:
1159 Improvements in Performance and Usability. *Mol. Biol. Evol.* **30**, 772–780 (2013).
- 1160 47. W. Li, A. Godzik, Cd-hit: a fast program for clustering and comparing large sets of
1161 protein or nucleotide sequences. *Bioinformatics* **22**, 1658–1659 (2006).
- 1162 48. M. N. Price, P. S. Dehal, A. P. Arkin, FastTree 2 – Approximately Maximum-Likelihood
1163 Trees for Large Alignments. *PLoS One* **5**, e9490 (2010).
- 1164 49. A. Rambaut, T. T. Lam, L. Max Carvalho, O. G. Pybus, Exploring the temporal structure
1165 of heterochronous sequences using TempEst (formerly Path-O-Gen). *Virus Evol.* **2**,
1166 vew007 (2016).
- 1167 50. B. Q. Minh, H. A. Schmidt, O. Chernomor, D. Schrempf, M. D. Woodhams, A. von
1168 Haeseler, R. Lanfear, IQ-TREE 2: New Models and Efficient Methods for Phylogenetic
1169 Inference in the Genomic Era. *Mol. Biol. Evol.* **37**, 1530–1534 (2020).
- 1170 51. M. Hasegawa, H. Kishino, T. Yano, Dating of the human-ape splitting by a molecular
1171 clock of mitochondrial DNA. *J. Mol. Evol.* **22**, 160–174 (1985).
- 1172 52. D. A. Duchêne, K. J. Tong, C. S. P. Foster, S. Duchêne, R. Lanfear, S. Y. W. Ho, Linking
1173 Branch Lengths across Sets of Loci Provides the Highest Statistical Support for
1174 Phylogenetic Inference. *Mol. Biol. Evol.* **37**, 1202–1210 (2020).
- 1175 53. P. Sagulenko, V. Puller, R. A. Neher, TreeTime: Maximum-likelihood phylodynamic
1176 analysis. *Virus Evol.* **4**, vex042 (2018).

- 1177 54. A. X. Han, E. Parker, S. Maurer-Stroh, C. A. Russell, Inferring putative transmission
1178 clusters with Phydely. *Virus Evol.* **5**, vez039 (2019).
- 1179 55. G. Yu, D. K. Smith, H. Zhu, Y. Guan, T. T.-Y. Lam, ggtree: an r package for visualization
1180 and annotation of phylogenetic trees with their covariates and other associated data.
1181 *Methods Ecol. Evol.* **8**, 28–36 (2017).
- 1182 56. P. Dixon, VEGAN, a package of R functions for community ecology. *J. Veg. Sci.* **14**,
1183 927–930 (2003).
- 1184 57. V. Hill, G. Baele, Bayesian Estimation of Past Population Dynamics in BEAST 1.10
1185 Using the Skygrid Coalescent Model. *Mol. Biol. Evol.* **36**, 2620–2628 (2019).
- 1186 58. A. Rambaut, A. J. Drummond, D. Xie, G. Baele, M. A. Suchard, Posterior Summarization
1187 in Bayesian Phylogenetics Using Tracer 1.7. *Syst. Biol.* **67**, 901–904 (2018).
- 1188 59. P. Lemey, A. Rambaut, A. J. Drummond, M. A. Suchard, Bayesian Phylogeography Finds
1189 Its Roots. *PLOS Comput. Biol.* **5**, e1000520 (2009).
- 1190 60. M. A. R. Ferreira, M. A. Suchard, Bayesian analysis of elapsed times in continuous-time
1191 Markov chains. *Can. J. Stat.* **36**, 355–368 (2008).
- 1192 61. D. Eddelbuettel, R. Francois, Rcpp: Seamless R and C++ Integration. *J. Stat. Softw.* **40**,
1193 1–18 (2011).
- 1194
1195

1196 Acknowledgments

1197
1198 We gratefully acknowledge the originating and submitting and laboratories that
1199 generated the sequence data that this study relies on.

1200 Funding:

1201
1202 This work was supported by US National Institutes of Health grant R01AI132362
1203 (SPJdJ, AC, CAR) and the Netherlands Organization for Scientific Research (NWO)
1204 Veni grant 9150162210121 (AXH).
1205
1206

1207 Author contributions:

1208
1209 Conceptualization: SPJdJ, CAR
1210 Methodology: SPJdJ, AC, AXH
1211 Investigation: SPJdJ
1212 Visualization: SPJdJ
1213 Supervision: AXH, CAR
1214 Writing—original draft: SPJdJ
1215 Writing—review & editing: SPJdJ, AC, AXH, CAR
1216

1217 Competing interests:

1218
1219 Authors declare that they have no competing interests.
1220

1221 Data and materials availability:

1222
1223 Sequence data is available from GISAID (accession numbers Table S1). All other data
1224 needed to evaluate the conclusions in the paper are present in the paper and/or the
1225 Supplementary Materials. Code is available at http://www.github.com/AMC-LAEB/usa_flu.
1226
1227

1228 **Supplementary Materials**

1229

1230 Figs. S1 to S11

1231 Table S1

1232